Bulk effective dielectric constant of a composite with a periodic microgeometry

David J. Bergman
School of Physics and Astronomy, Raymond and Beverly Sackler Faculty of Exact Sciences, Tel Aviv University, Tel Aviv 69978, Israel

Keh-Jim Dunn
Chevron Oil Field Research Co., P.O. Box 446, La Habra, California 90633
(Received 10 January 1992)

A method is presented for calculating the bulk effective dielectric constant of a two-component composite with a periodic microstructure. The method is based on a Fourier-space representation of an integral equation for the electric potential, which is used to produce a continued-fraction expansion for the dielectric constant. The method enabled us to include a much larger number of Fourier components in the calculation—up to 2×10^5 different values of reciprocal-lattice vectors—than some previously proposed Fourier methods. Consequently our method provides the possibility of performing reliable calculations of the dielectric constant of periodic composites that are neither dilute nor low contrast, and are not restricted to arrays of nonoverlapping spheres. We present results for a cubic array of nonoverlapping spheres, intended to serve as a test of quality, as well as results for a cubic array of overlapping spheres and a two-dimensional square array of prismatic inclusions for comparison with previous work.

I. INTRODUCTION

Recently, two different research groups proposed, independently and simultaneously, a method for calculating the bulk effective static dielectric constant $\epsilon_e(\epsilon_1, \epsilon_2)$ of a two-component composite medium with a periodic microgeometry.[1,2] In this method, Maxwell's equations are first transformed into equations for the Fourier coefficients of the fields. The space-dependent dielectric constant $\epsilon(\mathbf{r})$ is represented by its Fourier coefficients $\epsilon_{\mathbf{k}}$, which are nonzero only at reciprocal-lattice values of $\mathbf{k}$. Taking the static limit, the authors found that they needed to solve an infinite set of linear algebraic equations for the Fourier coefficients of the electric field at these same values of $\mathbf{k}$. The obvious advantage of this method over some previously developed ones[3–5] is that it is not limited to arrays of nonoverlapping spheres, but can tackle any kind of periodic microgeometry. Unfortunately, the method converges rather slowly with the number of Fourier components included in the calculation. Therefore it is quite difficult to get very accurate results when the system is not dilute and the contrast between the components, i.e., the ratio ϵ_1/ϵ_2, is very different from 1. In practice, the results for ϵ_e were often not better than those found by using the simple Clausius-Mossotti or Maxwell Garnett (MG) approximation, which ignores almost all the details of the microgeometry.[1]

In this article, we propose another method for calculating ϵ_e of such composites in the quasistatic regime. Our method also uses the Fourier coefficients of $\epsilon(\mathbf{r})$ at reciprocal-lattice values of $\mathbf{k}$, and is therefore applicable to quite general, periodic microgeometries. In our method, the periodicity is exploited in order to transform an integral equation for the electrostatic potential $\phi(\mathbf{r})$. This equation was introduced in Ref. 5, and at its heart lies an integral operator $\hat{\Gamma}$ which depends on the microgeometry through $\epsilon(\mathbf{r})$. The Fourier transform of this operator becomes a matrix of an infinite set of linear algebraic equations for the (reciprocal-lattice) Fourier coefficients of ϕ. But there are more efficient ways of using that matrix to obtain ϵ_e than simply solving those equations. These follow from the special analytic properties of $\epsilon_e(\epsilon_1, \epsilon_2)$. By exploiting these properties, we have been able to calculate ϵ_e by including reciprocal-lattice vectors in which all three components range over all integer values from -29 up to $+29$, altogether more than 2×10^5 different vectors. If we were to solve the equations for the Fourier coefficients of ϕ directly, even if we took full advantage of the point symmetry of a cubic lattice, we could only have reduced the total number of Fourier coefficients (and equations for them) by a factor of 16. That would leave about 13 000 equations to be solved simultaneously, with a matrix that is not sparse—far beyond the capability of even the largest computers today. By contrast, our method makes quite modest use of both memory and CPU time, and can easily be used to calculate even more Fourier coefficients of ϕ.

The rest of this article is organized as follows: In Sec. II we present our method along with a short summary of the theory which underlies it. In Sec. III A we present numerical results for a simple cubic array of nonoverlapping spheres [Fig.1(a)] calculated using our method. For comparison, we also calculated the same results using the method of Ref. 5, which is more accurate for this type of system. In Sec. III B we present numerical results for a cubic array of overlapping spheres and a two-dimensional (2D) square array of prismatic inclusions [Fig.1(b)] for comparison with previous work.

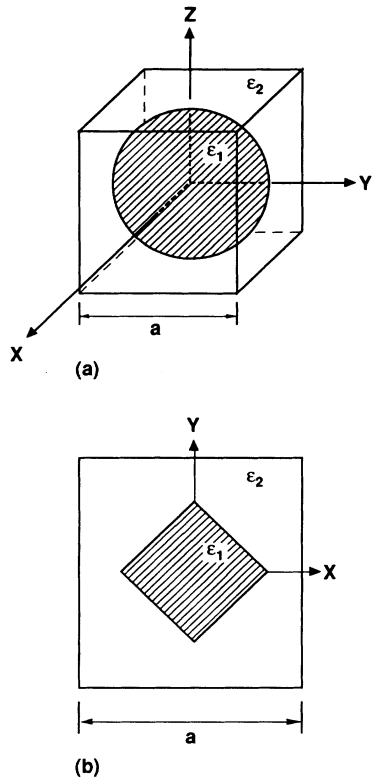

FIG. 1. (a) Unit cell of a simple 3D cubic lattice of identical spheres with dielectric constant ϵ_1 embedded in a host material with dielectric constant ϵ_2. (b) Unit cell of a simple 2D square lattice of square or prismatic inclusions ϵ_1 in an ϵ_2 host.

II. THEORY OF THE METHOD

A. Summary of the underlying theory

This is a summary of a more extensive discussion which can be found elsewhere.[5–7] Consider a sample of our medium that fills up the entire volume in between the plates of an infinite, parallel plate capacitor of thickness L, taken to lie perpendicular to the z axis. In order to calculate ϵ_e, we first use an integral equation for the potential $\phi(\mathbf{r})$

$$\phi(\mathbf{r}) = z + \frac{1}{s}\hat{\Gamma}\phi, \tag{2.1}$$

where

$$s \equiv \frac{\epsilon_2}{\epsilon_2 - \epsilon_1}, \tag{2.2}$$

$$\hat{\Gamma}\phi \equiv \int dV' \theta_1(\mathbf{r}')\nabla' G(\mathbf{r},\mathbf{r}') \cdot \nabla' \phi(\mathbf{r}'). \tag{2.3}$$

The linear operator $\hat{\Gamma}$ depends on the microgeometry through $\theta_1(\mathbf{r})$, the characteristic function which defines the domain of the ϵ_1 component, but is independent of the physical moduli of the components ϵ_1, ϵ_2. This operator is made self-adjoint by defining the scalar product of two (scalar) functions as follows:

$$\langle \phi | \psi \rangle \equiv \frac{1}{V} \int dV \theta_1 \nabla \phi^* \cdot \nabla \psi. \tag{2.4}$$

The dielectric constant ϵ_e is now calculated from

$$F(s) \equiv 1 - \frac{\epsilon_e}{\epsilon_2} = \frac{1}{s}\langle z | \phi \rangle = \left\langle z \left| \frac{1}{s - \hat{\Gamma}} \right| z \right\rangle, \tag{2.5}$$

where we have substituted the symbolic solution of (2.1), $\phi = s(s - \hat{\Gamma})^{-1} z$, in order to get the final result.

Because $\hat{\Gamma}$ has a complete set of eigenfunctions ϕ_n with real eigenvalues s_n

$$\hat{\Gamma}\phi_n = s_n \phi_n, \tag{2.6}$$

therefore (2.5) can be transformed into

$$F(s) = \sum \frac{F_n}{s - s_n}, \tag{2.7}$$

where

$$F_n = \frac{|\langle z | \phi_n \rangle|^2}{\langle \phi_n | \phi_n \rangle} \geq 0. \tag{2.8}$$

The following inequalities are also satisfied:

$$0 \leq s_n < 1, \quad F(1) \leq 1, \quad \sum F_n \leq 1. \tag{2.9}$$

Another useful representation for $F(s)$ is obtained by expanding it in powers of $1/s$. When this is done by starting from (2.7), the expansion coefficients are obtained as the moments of the pole spectrum, weighted by the residues F_n

$$F(s) = \frac{\sum F_n}{s} + \frac{\sum s_n F_n}{s^2} + \ldots + \frac{\sum s_n^{r-1} F_n}{s^r} + \ldots . \tag{2.10}$$

By comparing this to a similar expansion of (2.5), we find that

$$\sum_n s_n^r F_n = \langle z | \hat{\Gamma}^r | z \rangle. \tag{2.11}$$

The zero moment is thus given by

$$\sum F_n = \langle z | z \rangle = \frac{V_1}{V} = p_1, \tag{2.12}$$

i.e., the volume fraction of the ϵ_1 component. The first moment can also be calculated quite generally if the microgeometry is either isotropic or cubic[5,6]

$$\sum s_n F_n = \tfrac{1}{3} p_1 (1 - p_1). \tag{2.13}$$

To calculate higher-order moments we need to use more detailed information about the microgeometry. In order to use (2.11) for calculating those moments, we need to have a useful representation of the operator $\hat{\Gamma}$.

Elementary bounds for $F(s)$ are easily obtained from its general properties. For real values of s, these are[6]

$$F(s) \in (0, 1/s) \text{ for real } s \text{ outside } (0,1). \tag{2.14}$$

For complex values of s, $F(s)$ must lie above the

straight line through 0 and $1/s$ in the complex F plane, and also on the inside of the circle through the three points 0, 1, and $1/s$. This is both a rigorous and an optimal bound with the given information. It is a lens-shaped region defined by the straight line segment and circular arc with the following parametric representations:[7]

$$\frac{s_0}{s}, \quad \frac{1-s_0}{s-s_0}, \quad 0 \le s_0 \le 1. \tag{2.15}$$

In Sec. II C we will show that the elementary bounds of (2.14) and (2.15) can be expanded into progressively tighter bounds by including increasing amounts of information about the terms of the series (2.10).

B. Fourier representation of the problem for a periodic composite medium

First we subtract from $\phi(\mathbf{r})$ the simple linear function z

$$\psi(\mathbf{r}) \equiv \phi - z = \frac{1}{s}(\hat{\Gamma}z + \hat{\Gamma}\psi) = \frac{\hat{\Gamma}}{s-\hat{\Gamma}}z. \tag{2.16}$$

The remaining function $\psi(\mathbf{r})$ is clearly periodic since $\hat{\Gamma}z$ is periodic, as is $\hat{\Gamma}f$ for any periodic function $f(\mathbf{r})$. We can therefore represent ψ by a Fourier series

$$\psi(\mathbf{r}) = \sum_{\mathbf{g}} \psi_{\mathbf{g}} e^{i\mathbf{g}\cdot\mathbf{r}}, \tag{2.17}$$

where the sum is over all the vectors $\mathbf{g}$ of the appropriate reciprocal lattice. The Fourier coefficients of $\psi(\mathbf{r})$ are given by

$$\psi_{\mathbf{g}} = \frac{1}{V_a}\int_{V_a} dV \psi(\mathbf{r}) e^{-i\mathbf{g}\cdot\mathbf{r}}, \tag{2.18}$$

where V_a is the volume of the unit cell of the periodic composite.

It is now just a matter of some straightforward algebra to transform any equation from Sec. II A into an equation involving Fourier coefficients. In this way we get, for any nonzero reciprocal-lattice vector $\mathbf{g}$,

$$i|\mathbf{g}|(\hat{\Gamma}z)_{\mathbf{g}} = \cos(\mathbf{g},\mathbf{e}_z)\theta_{\mathbf{g}} \tag{2.19}$$

$$i|\mathbf{g}|(\hat{\Gamma}f)_{\mathbf{g}} = \sum_{\mathbf{g}'\neq 0} \Gamma_{\mathbf{g}\mathbf{g}'}\, i|\mathbf{g}'|f_{\mathbf{g}'}, \tag{2.20}$$

where $\theta_{\mathbf{g}} = \theta^*_{-\mathbf{g}}$ is the Fourier coefficient of $\theta_1(\mathbf{r})$, $\mathbf{e}_z$ is the unit vector along the z axis, $(\mathbf{g},\mathbf{e}_z)$ indicates the angle between $\mathbf{g}$ and $\mathbf{e}_z$, $f(\mathbf{r})$ is any periodic function, and

$$\Gamma_{\mathbf{g}\mathbf{g}'} \equiv \cos(\mathbf{g},\mathbf{g}')\theta_{\mathbf{g}-\mathbf{g}'} \tag{2.21}$$

is a matrix which represents the operator $\hat{\Gamma}$ in this scheme. For $\mathbf{g} = 0$ the right-hand side of these equations is replaced by 0.

The integral equation (2.1) or (2.16) transforms into an infinite set of linear algebraic equations for $\psi_{\mathbf{g}}$. In order to simplify it, we define new coefficients

$$a_{\mathbf{g}} \equiv i|\mathbf{g}|\psi_{\mathbf{g}} \quad \text{for} \quad \mathbf{g} \neq 0. \tag{2.22}$$

These satisfy the following equations:

$$sa_{\mathbf{g}} = \cos(\mathbf{g},\mathbf{e}_z)\theta_{\mathbf{g}} + \sum_{\mathbf{g}'\neq 0} \Gamma_{\mathbf{g}\mathbf{g}'}a_{\mathbf{g}'}. \tag{2.23}$$

The scalar product of two arbitrary periodic functions $\psi^{(1)}$, $\psi^{(2)}$ can now be calculated from

$$\langle\psi^{(1)}|\psi^{(2)}\rangle = \sum_{\mathbf{g}\neq 0}\sum_{\mathbf{g}'\neq 0} a^{(1)*}_{\mathbf{g}}\Gamma_{\mathbf{g}\mathbf{g}'}a^{(2)}_{\mathbf{g}'}, \tag{2.24}$$

while the scalar product of z with an arbitrary periodic function ψ is calculated from

$$\langle z|\psi\rangle = \sum_{\mathbf{g}\neq 0} \cos(\mathbf{g},\mathbf{e}_z)\theta_{-\mathbf{g}}a_{\mathbf{g}}. \tag{2.25}$$

Using the solution of (2.23), $F(s)$ could be calculated from

$$sF(s) - p_1 = \langle z|\psi\rangle = \sum_{\mathbf{g}\neq 0} \cos(\mathbf{g},\mathbf{e}_z)\theta_{-\mathbf{g}}a_{\mathbf{g}}. \tag{2.26}$$

Another expression for this quantity is obtained by using (2.23) to replace the factor $\cos(\mathbf{g},\mathbf{e}_z)\theta_{-\mathbf{g}}$ in (2.26). This yields

$$sF(s) - p_1 = -s\sum_{\mathbf{g}\neq 0} a_{-\mathbf{g}}a_{\mathbf{g}} + \sum_{\mathbf{g}\neq 0}\sum_{\mathbf{g}'\neq 0}\Gamma_{\mathbf{g}\mathbf{g}'}a_{-\mathbf{g}}a_{\mathbf{g}'}. \tag{2.27}$$

Although this expression is more complicated to evaluate than (2.26), it is useful to combine the two expressions to get

$$sF(s) - p_1 = s\sum_{\mathbf{g}\neq 0} a_{-\mathbf{g}}a_{\mathbf{g}} - \sum_{\mathbf{g}\neq 0}\sum_{\mathbf{g}'\neq 0}\Gamma_{\mathbf{g}\mathbf{g}'}a_{-\mathbf{g}}a_{\mathbf{g}'} + 2\sum_{\mathbf{g}\neq 0}\cos(\mathbf{g},\mathbf{e}_z)\theta_{-\mathbf{g}}a_{\mathbf{g}}. \tag{2.28}$$

The last expression is better than the previous two because it has a variational property: If we consider it as a quadratic form in the coefficients $a_{\mathbf{g}}$, then it is stationary when these coefficients solve (2.23). Moreover, using the fact that $a_{-\mathbf{g}} = -a^*_{\mathbf{g}}$, and the fact that the eigenvalues of the matrix $\Gamma_{\mathbf{g}\mathbf{g}'}$ are just the eigenvalues s_n of $\hat{\Gamma}$, it is easy to show that this form is positive (negative) definite for real values of s when $s < 0$ ($s > 1$). In those cases, the quadratic form achieves its minimum (maximum) value at the solution of (2.23). If that solution is known approximately, then use of (2.28) will lead to a more accurate result for $F(s)$ than either (2.26) or (2.27).

Another way to obtain $F(s)$ is by solving the homogeneous version of (2.23) for the eigenvectors $a^{(n)}_{\mathbf{g}}$ and eigenvalues s_n of the matrix $\Gamma_{\mathbf{g}\mathbf{g}'}$

$$s_n a^{(n)}_{\mathbf{g}} = \sum_{\mathbf{g}'\neq 0}\Gamma_{\mathbf{g}\mathbf{g}'}a^{(n)}_{\mathbf{g}'}. \tag{2.29}$$

Those can then be used to produce the pole expansion (2.7) for $F(s)$, or a variant of it for $sF(s) - p_1$

$$sF(s) - p_1 = \sum \frac{s_n F_n}{s - s_n}. \tag{2.30}$$

Noting that the relevant eigenfunctions of $\hat{\Gamma}$ (that means those eigenfunctions whose scalar product with z is nonzero, see Ref. 5) are themselves periodic, it is easy to show, starting from (2.8), that the residues in this expansion are given by

$$s_n F_n = \frac{\left| \sum_{\mathbf{g}\neq 0} \cos(\mathbf{g},\mathbf{e}_z)\theta_{-\mathbf{g}} a_{\mathbf{g}}^{(n)} \right|^2}{\sum_{\mathbf{g}\neq 0} |a_{\mathbf{g}}^{(n)}|^2}. \tag{2.31}$$

Finally, we can use the matrix $\Gamma_{\mathbf{g}\mathbf{g}'}$ to evaluate the moments of the pole spectrum of $F(s)$ from (2.11) for use in the series expansion (2.10). From (2.19), (2.20) and (2.25) it is not difficult to get

$$\langle z|\hat{\Gamma}^r|z\rangle = \sum_{\mathbf{g}\neq 0}\sum_{\mathbf{g}'\neq 0} \cos(\mathbf{g},\mathbf{e}_z)\theta_{-\mathbf{g}}(\Gamma^{r-1})_{\mathbf{g}\mathbf{g}'}\cos(\mathbf{g}',\mathbf{e}_z)\theta_{\mathbf{g}'} \quad \text{for } r \geq 1, \tag{2.32}$$

where the factor $(\Gamma^{r-1})_{\mathbf{g}\mathbf{g}'}$ denotes the matrix of (2.21) raised to the power $r-1$.

If we want to use very large matrices $\Gamma_{\mathbf{g}\mathbf{g}'}$, this is the best method to use because we can avoid having to store this matrix in memory. All we need to do is to keep in memory the vector $\theta_{\mathbf{g}}$ of Fourier coefficients of θ_1. From that we can construct the vector $\cos(\mathbf{g},\mathbf{e}_z)\theta_{\mathbf{g}}$, and multiply it iteratively by the matrix $\Gamma_{\mathbf{g}\mathbf{g}'}$ whose elements are recalculated, when needed, by using (2.21).

The moments calculated from (2.32) using a truncated, finite-size portion of the matrix $\Gamma_{\mathbf{g}\mathbf{g}'}$ turn out to converge rather slowly with increasing size. Therefore an extrapolation of the results to infinite size is usually called for, as noted also in Ref. 1. In evaluating the merits of different types of extrapolation procedures for the moments, a useful test is the precise value of the first moment in the case of a microstructure with cubic symmetry (2.13), which generalizes to

$$\langle z|\hat{\Gamma}|z\rangle = \frac{1}{d}p_1(1-p_1) \tag{2.33}$$

for a hypercubic microstructure when the effective dimensionality of the composite is d (actually, in two dimensions this result holds for both square and triangular symmetries).[6]

C. Rigorous bounds from the series for $F(s)$

The power series of (2.10) may at first seem useless outside its radius of convergence. However, due to the special properties of $F(s)$, that series can be transformed into a continued fraction that converges everywhere except for its singular points, which are all on the semiclosed real segment [0,1). If that fraction is terminated appropriately, the result is always a rigorous bound for $F(s)$. There are standard methods for handling this.[8] Here we will outline briefly the main steps.

In order to show these properties, and also to obtain an explicit construction of the continued fraction, we first define a hierarchy of functions $C^{(r)}(s)$ that have the same properties as $F(s)$, namely, they have a pole expansion like (2.7) and satisfy inequalities like (2.8) and (2.9) (Ref. 9).

$$C^{(0)}(s) \equiv F(s) \tag{2.34}$$

$$C^{(r+1)}(s) \equiv \frac{1-\mu_r/sC^{(r)}(s)}{1-\mu_r} \tag{2.35}$$

$$\mu_r \equiv \sum_n C_n^{(r)}, \quad 0 < \mu_r < 1 \tag{2.36}$$

$$C^{(r)}(s) = \sum_n \frac{C_n^{(r)}}{s - c_n^{(r)}}. \tag{2.37}$$

All of these properties are easily proven by induction on the index r.

By inverting these definitions, one can express $F(s)$ as a continued fraction that depends on s and on the zero moments of $C^{(r)}(s)$, i.e., on μ_r, $r = 0 \ldots n-1$, and terminates with $C^{(n)}(s)$ itself

$$F(s) = \cfrac{\mu_0}{s-(1-\mu_0)\mu_1 -} \cfrac{(1-\mu_0)\mu_1(1-\mu_1)\mu_2}{s-(1-\mu_1)\mu_2-(1-\mu_2)\mu_3 -} \cfrac{(1-\mu_2)\mu_3(1-\mu_3)\mu_4}{s-(1-\mu_3)\mu_4-(1-\mu_4)\mu_5 -} \cdots \begin{cases} \cfrac{(1-\mu_{n-2})\mu_{n-1}(1-\mu_{n-1})}{1/C^{(n)}(s)-(1-\mu_{n-1})} & \text{for even } n \\ \cfrac{(1-\mu_{n-3})\mu_{n-2}(1-\mu_{n-2})\mu_{n-1}}{s-(1-\mu_{n-2})\mu_{n-1}-(1-\mu_{n-1})sC^{(n)}(s)} & \text{for odd } n. \end{cases} \tag{2.38}$$

It is also straightforward to relate the moments of $C^{(r+1)}(s)$ to those of $C^{(r)}(s)$—these are the coefficients of the expansion in powers of $1/s$, like (2.10). The nth moment of $C^{(r+1)}(s)$ depends on the moments of $C^{(r)}(s)$ up to order $n+1$. Therefore, if one begins with a certain finite number of known moments of $C^{(0)}(s) \equiv F(s)$, the number decreases as one ascends the hierarchy until a value of r is reached for which nothing is known about the series for $C^{(r)}(s)$—not even its zero moment μ_r. At that point, the hierarchy is terminated naturally. We can replace the last $C^{(r)}(s)$ by the elementary bounds of (2.14) or (2.15). In this way we obtain bounds for $F(s)$ which take into account all the information that was available about its moments.

To construct these bounds, we must be able to translate the known moments of $C^{(r)}(s)$ into a set of (one less) moments of $C^{(r+1)}(s)$. This is achieved by using the following formulas:

$$sC^{(r)}(s) \equiv \mu_r \left(1 + \sum_{i=1}^{\infty} a_i/s^i\right)$$

$$sC^{(r+1)}(s) \equiv \mu_{r+1} \left(1 + \sum_{i=1}^{\infty} b_i/s^i\right)$$

$$\mu_{r+1} = \frac{a_1}{1-\mu_r}, \quad b_i = \frac{\alpha_{i+1}}{\alpha_1}, \quad i > 0 \qquad (2.39)$$

$$\alpha_1 = a_1$$

$$\alpha_j = a_j - \sum_{i=1}^{j-1} \alpha_i a_{j-i}.$$

If we know the first $n+1$ moments of $C^{(0)}(s) \equiv F(s)$, we can use these formulas repetitiously to calculate the zero moments of the $C^{(r)}(s)$, μ_r, up to $r = n$.

In practice, when r increases, μ_r becomes increasingly sensitive to the accuracy of the *low-order* moments of $F(s)$. At some point this leads to a value of μ_r which lies outside the range [0,1]. When this occurs we terminate the procedure at the previous value of r.

III. NUMERICAL RESULTS

A. Simple cubic array of nonoverlapping spheres

This system was chosen in order to test our approach: The Fourier coefficients of $\theta_1(\mathbf{r})$ are easily calculable in closed form

$$\theta_{\mathbf{g}} = \frac{4\pi}{(|\mathbf{g}|a)^3}[\sin(|\mathbf{g}|R) - |\mathbf{g}|R\cos(|\mathbf{g}|R)], \qquad (3.1)$$

where R is the radius of the spheres, a is the linear size of the unit cell, and

$$\mathbf{g} = \frac{2\pi}{a}(n_x, n_y, n_z) \quad (n_x, n_y, n_z = \text{integers}) \qquad (3.2)$$

is the reciprocal-lattice vector. For a reciprocal lattice of finite size N; n_x, n_y, and n_z vary from $-N$ to $+N$.

We then used the procedure described in Sec. II B to calculate the first 20 moments of $F(s)$ for $p_1 = 4\pi R^3/3a^3 = 0.5$. For comparison we also calculated the same moments using a different matrix representation for the operator $\hat{\Gamma}$—the one obtained by using the individual grain eigenfunctions as a basis in Hilbert space.[5] For the case of spherical grains, those eigenfunctions are essentially the spherical harmonics. The results from both computations are exhibited in Table I.

The second method is much faster and more accurate for this problem, and probably all the digits exhibited in the table (last column) are significant: Two calculations were performed using this method, i.e., $l_{\max}=25$ and $l_{\max}=49$, where $l_{\max}$ is the maximum order of the spherical harmonics that were included in the calculation. The fractional difference between results of $l_{\max}=25$ and 49 is about 3×10^{-5} for the 10th moment, and about 3×10^{-3} for the 20th moment. Only the results of $l_{\max}=49$ are listed in Table I. These results were used as a benchmark to check our Fourier-expansion results and the various methods of extrapolation that we tried out on them. Calculations using the Fourier method were carried out for many different sizes of the truncated reciprocal lattice between $N=5$ and $N=29$. The first two columns of

TABLE I. Moments of $F(s)$ for a simple cubic array of nonoverlapping spheres computed by Fourier expansion over the reciprocal lattice and by expansion over the basis of the individual sphere eigenfunctions (Ref. 5). $p_1=0.5$.

Order	Fourier ($N=25$)	Fourier ($N=27$)	Fourier (extrapolated)	Sphere eigenfunctions
0	0.500000	0.500000	0.500000	0.500000
1	0.816581×10^{-1}	0.817815×10^{-1}	0.833330×10^{-1}	0.833333×10^{-1}
2	0.238951×10^{-1}	0.238650×10^{-1}	0.235449×10^{-1}	0.235424×10^{-1}
3	0.947469×10^{-2}	0.946023×10^{-2}	0.928714×10^{-2}	0.925032×10^{-2}
4	0.451570×10^{-2}	0.450458×10^{-2}	0.427436×10^{-2}	0.435191×10^{-2}
5	0.241389×10^{-2}	0.240501×10^{-2}	0.223432×10^{-2}	0.228715×10^{-2}
6	0.139654×10^{-2}	0.138953×10^{-2}	0.128166×10^{-2}	0.129546×10^{-2}
7	0.856710×10^{-3}	0.851016×10^{-3}	0.778887×10^{-3}	0.773883×10^{-3}
8	0.550033×10^{-3}	0.545255×10^{-3}	0.493259×10^{-3}	0.480848×10^{-3}
9	0.366386×10^{-3}	0.362283×10^{-3}	0.322131×10^{-3}	0.307884×10^{-3}
10	0.251711×10^{-3}	0.248139×10^{-3}	0.215194×10^{-3}	0.201841×10^{-3}
11	0.177613×10^{-3}	0.174479×10^{-3}	0.146004×10^{-3}	0.134849×10^{-3}
12	0.128343×10^{-3}	0.125581×10^{-3}	0.998792×10^{-4}	0.914929×10^{-4}
13	0.947647×10^{-4}	0.923230×10^{-4}	0.683065×10^{-4}	0.628719×10^{-4}
14	0.713805×10^{-4}	0.692177×10^{-4}	0.461744×10^{-4}	0.436653×10^{-4}
15	0.547774×10^{-4}	0.528587×10^{-4}	0.303253×10^{-4}	0.305978×10^{-4}
16	0.427794×10^{-4}	0.410752×10^{-4}	0.187649×10^{-4}	0.216033×10^{-4}
17	0.339670×10^{-4}	0.324517×10^{-4}	0.102173×10^{-4}	0.153508×10^{-4}
18	0.273952×10^{-4}	0.260463×10^{-4}	0.385414×10^{-5}	0.109677×10^{-4}
19	0.224232×10^{-4}	0.212213×10^{-4}	-0.863165×10^{-6}	0.787299×10^{-5}
20	0.186098×10^{-4}	0.175378×10^{-4}	-0.429039×10^{-5}	0.567431×10^{-5}

Table I show the directly calculated results for reciprocal-lattice sizes N=25 and 27, while the third column shows the results for the infinite reciprocal lattice as obtained by nonlinear extrapolation from the finite lattice results up to $N = 27$. The Fourier-expansion results converge quite slowly with increasing N, and even when carefully extrapolated to infinite N they are evidently less accurate than the results from the second method for an array of nonoverlapping spheres.

The two sets of moments of $F(s)$, i.e., obtained by the Fourier method and by eigenfunctions of a sphere, were then processed as described in Sec. II C to obtain the zero moments μ_r of $C^{(r)}(s)$ up to the point where μ_r first excurses outside the real segment [0,1]. The lower order μ_r's were then used to produce upper and lower bounds for $F(s)$. All of these results are exhibited in Table II. Notice that as r increases the upper and lower bounds alternate because of (2.35). It is evident that as more and more of the acceptable μ_r's are used, the bounds get tighter at both ends. This is in agreement with similar results obtained for this case in Ref. 10, where an approach was used that is essentially equivalent to the continued fraction method used here. One should of course remember that although the bounds produced by this method are rigorous, they will always reflect whatever errors exist in the numerical values of the μ_r's.

It is useful to note that in Table II, and in Tables III, IV, V, VII and X as well, the bounds in the second row (i.e., the $r = 1$ row) are the Hashin-Shtrikman bounds.[11] In that same row, the so-called bound 1 is the same as the result of the Clausius-Mossotti or Maxwell Garnett approximation (MG) (see, e.g., Ref. 12). It is also worthwhile to mention that the upper bounds on $sF(s)$ always correspond to a system in which the inclusions (i.e., the ϵ_1 component) form a percolating network, whereas the lower bounds correspond to a system where the inclusions do not percolate. For this reason, the upper bounds for $F(s)$ in Tables II–V are probably closer to the correct results than are the lower bounds (note that both s and $F(s)$ in these tables are always negative numbers, and that the nonoverlapping spheres are also nonpercolating), while in Table VII it is the lower bounds that are probably closer to the truth.

It seems the accuracy of the final result for $F(s)$, and hence ϵ_e, depends on the accuracy of the computed moments and also largely on how the extrapolation to the reciprocal lattice of infinite size is done. Of greatest importance is the accuracy of the low-order moments of $F(s)$. Various methods of extrapolation have been tried. The nonlinearly extrapolated moments using the form

$$y = A + \frac{B}{N^{\alpha}} \tag{3.3}$$

produce better results than moments obtained by linear extrapolation [i.e., putting $\alpha = 1$ in (3.3)] from the two largest reciprocal-lattice sizes. On the other hand, the value of $F(s)$ obtained by linearly extrapolating the *bounds* calculated from the two largest reciprocal lattice sizes is slightly better than that obtained from nonlinearly extrapolated moments. The linear and nonlinear extrapolations of zero moments of $C^{(r)}(s)$, i.e., μ_r, computed at finite reciprocal-lattice sizes, produce the best results for $F(s)$ when s is real and outside the segment (0,1), with the latter slightly better than the former. Both results are shown in Table III using the same parameters s, p_1 that were used in Table I. The fact that

TABLE II. Bounds on $F(s)$ for a simple cubic array of nonoverlapping spheres computed by the continued fraction method using moments of $F(s)$ obtained from the Fourier-expansion method and the method of Ref. 5. The bounds in each row r are obtained by using the zero moments of $C^{(q)}(s)$ for all $0 \leq q \leq r$. Bound 1 is then obtained by substituting 0 for $C^{(r+1)}(s)$, while bound 2 is obtained by taking $C^{(r+1)}(s) \rightarrow 1/s$. s=−0.5, i.e., ϵ_1/ϵ_2=3. p_1=0.5.

	Fourier (extrapolated)			Eigenfunctions of sphere		
r	μ_r	Bound 1	Bound 2	μ_r	Bound 1	Bound 2
0	0.500000	-0.100000	-0.500000	0.500000	-0.100000	-0.500000
1	0.333333	-0.750000	-0.875000	0.333333	-0.750000	-0.875000
2	0.173897	-0.787034	-0.765383	0.173764	-0.787010	-0.765370
3	0.329676	-0.775296	-0.780907	0.325892	-0.775370	-0.780961
4	0.120971	-0.776467	-0.775750	0.173692	-0.776980	-0.776034
5	0.830597	-0.775802	-0.775887	0.387486	-0.776408	-0.776660
6				0.143312	-0.776466	-0.776431
7				0.441329	-0.776442	-0.776452
8				0.115104	-0.776444	-0.776443
9				0.461968	-0.776443	-0.776444
10				0.081555	-0.776443	-0.776443
11				0.479343	-0.776443	-0.776443
12				0.060438	-0.776443	-0.776443
13				0.481049	-0.776443	-0.776443
14				0.040697	-0.776443	-0.776443
15				0.488268	-0.776443	-0.776443
16				0.028974	-0.776443	-0.776443
17				0.488238	-0.776443	-0.776443
18				0.003933	-0.776443	-0.776443

TABLE III. Bounds on $F(s)$ for a simple cubic array of nonoverlapping spheres computed by the continued fraction method using zero moments of $C^{(r)}(s)$, i.e., μ_r, obtained from linear and nonlinear extrapolations of zero moments of $C^{(r)}(s)$ calculated at finite reciprocal-lattice sizes. $s=-0.5$, $\epsilon_1/\epsilon_2=3$. $p_1=0.5$.

	Linear extrapolation			Nonlinear extrapolation		
r	μ_r	Bound 1	Bound 2	μ_r	Bound 1	Bound 2
0	0.500000	-0.100000	-0.500000	0.500000	-0.100000	-0.500000
1	0.333333	-0.750000	-0.875000	0.333333	-0.750000	-0.875000
2	0.172990	-0.786869	-0.765298	0.173895	-0.787034	-0.765383
3	0.333891	-0.775067	-0.780677	0.330815	-0.775269	-0.780884
4	0.150927	-0.776487	-0.775636	0.130767	-0.776524	-0.775760
5	0.456839	-0.775911	-0.776137	0.248539	-0.776174	-0.776356
6	0.308176	-0.775922	-0.775915	0.321207	-0.776264	-0.776219
7	0.610847	-0.775916	-0.775918	0.389455	-0.776239	-0.776251
8	0.592070	-0.775916	-0.775916	0.244676	-0.776243	-0.776241
9	0.750967	-0.775916	-0.775916	0.562156	-0.776242	-0.776242

TABLE IV. Bounds on $F(s)$ for a simple cubic array of nonoverlapping spheres for various values of s computed by the continued fraction method using Fourier expansion and linearly extrapolated zero moments of $C^{(r)}(s)$. $p_1=0.5$.

		$s=-0.1$ ($\epsilon_1/\epsilon_2=11$)		$s=-0.01$ ($\epsilon_1/\epsilon_2=101$)		$s=-0.001$ ($\epsilon_1/\epsilon_2=1001$)	
r	μ_r	Bound 1	Bound 2	Bound 1	Bound 2	Bound 1	Bound 2
0	0.500000	-5.000000	-0.833333	-50.00000	-0.980392	-500.0000	-0.998004
1	0.333333	-1.875000	-4.107143	-2.830189	-40.11858	-2.982107	-400.1199
2	0.172990	-2.818460	-2.014291	-21.46052	-3.195223	-205.5288	-3.394640
3	0.333891	-2.197258	-2.628793	-3.882335	-17.76905	-4.212637	-165.6389
4	0.150927	-2.356047	-2.218949	-10.24824	-3.997746	-80.54748	-4.357177
5	0.456839	-2.238105	-2.306848	-4.129635	-8.280875	-4.528317	-57.12979
6	0.030818	-2.242974	-2.238578	-4.503215	-4.133696	-9.449933	-4.533741
7	0.610847	-2.238835	-2.240359	-4.136237	-4.285772	-4.537190	-6.562739
8	0.059207	-2.238973	-2.238848	-4.150594	-4.136394	-4.733115	-4.537407
9	0.750967	-2.238852	-2.238881	-4.136445	-4.140202	-4.537478	-4.589958

TABLE V. Bounds on $F(s)$ for a simple cubic array of nonoverlapping spheres for various values of s computed by the continued fraction method using moments of $F(s)$ obtained from eigenfunctions of a sphere. $p_1=0.5$.

		$s=-0.1$ ($\epsilon_1/\epsilon_2=11$)		$s=-0.01$ ($\epsilon_1/\epsilon_2=101$)		$s=-0.001$ ($\epsilon_1/\epsilon_2=1001$)	
r	μ_r	Bound 1	Bound 2	Bound 1	Bound 2	Bound 1	Bound 2
0	0.500000	-5.000000	-0.833333	-50.00000	-0.980392	-500.0000	-0.998004
1	0.333333	-1.875000	-4.107143	-2.830189	-40.11858	-2.982107	-400.1199
2	0.173764	-2.821405	-2.014998	-21.51090	-3.197182	-206.0651	-3.396873
3	0.325892	-2.203936	-2.636697	-3.912333	-17.92302	-4.249463	-167.3053
4	0.173692	-2.382535	-2.229921	-11.02475	-4.053914	-89.45524	-4.427552
5	0.387486	-2.258458	-2.339300	-4.266569	-9.356326	-4.707551	-69.71449
6	0.143312	-2.284680	-2.261839	-6.322407	-4.300489	-31.87943	-4.754157
7	0.441329	-2.265044	-2.276509	-4.341855	-5.672171	-4.812925	-23.33183
8	0.115104	-2.267774	-2.265360	-4.719358	-4.347054	-10.21547	-4.820542
9	0.461968	-2.265648	-2.266803	-4.352930	-4.577243	-4.829386	-8.174791
10	0.081555	-2.265836	-2.265668	-4.394719	-4.353437	-5.464571	-4.830170
11	0.479343	-2.265685	-2.265762	-4.353975	-4.377016	-4.831018	-5.193510
12	0.060438	-2.265694	-2.265686	-4.356946	-4.354008	-4.878395	-4.831073
13	0.481049	-2.265687	-2.265691	-4.354044	-4.355633	-4.831131	-4.857277
14	0.040697	-2.265687	-2.265687	-4.354180	-4.354045	-4.833398	-4.831134
15	0.488268	-2.265687	-2.265687	-4.354047	-4.354117	-4.831136	-4.832344
16	0.028974	-2.265687	-2.265687	-4.354051	-4.354047	-4.831209	-4.831136
17	0.488238	-2.265687	-2.265687	-4.354047	-4.354049	-4.831136	-4.831175
18	0.003933	-2.265687	-2.265687	-4.354047	-4.354047	-4.831137	-4.831136

TABLE VI. Comparison of our results with those of Tao, Chen, and Sheng (Ref. 1) and with results of the simple Maxwell-Garnett or Clausius-Mossotti approximation in the case of a simple cubic array of spheres, both overlapping and nonoverlapping. $s=-0.5$, i.e., $\epsilon_1/\epsilon_2=3$.

p_1	Present method	Tao, Chen, and Sheng	MG
0.1	1.1250	1.126	1.125
0.3	1.4112	1.404	1.409
0.5	1.7759	1.797	1.750
0.52	1.8292	1.841	1.788
0.672	2.1707	2.175	2.103
0.738	2.3290	2.334	2.257
0.798	2.4765	2.479	2.406
0.896	2.7262	2.732	2.676

the index r now goes up to 9 (as compared to 5 in Table II) before μ_r excurses outside the real segment [0,1] is another indication that these results are better than the extrapolated Fourier-expansion results of Table II. The linear extrapolation of μ_r does better in producing bounds for $F(s)$ at complex values of s than does the nonlinear extrapolation of μ_r. Results of calculations for the first ten moments of $F(s)$ using the reciprocal lattice of size $N=29$ were also included in the data analysis in Tables II and III.

As a more severe test, we also computed bounds for $F(s)$ at values of s that are very close to zero. This corresponds to large values of the contrast ϵ_1/ϵ_2. Results from the Fourier-expansion method, using linearly extrapolated zero moments of $C^{(r)}(s)$, as well as results obtained by using eigenfunctions of spheres, are listed in Tables IV and V, respectively. Notice that as the contrast increases, the same number of moments μ_r leads to pairs of bounds that are progressively less tight. The quality of the agreement between the two sets of results also deteriorates. Nevertheless, even at $\epsilon_1/\epsilon_2 = 1001$, the Fourier method with linear extrapolation of μ_r errs by only about 6%.

Finally, as the most stringent test of our method we also tried to use it to evaluate $\mathrm{Im}[F(s)]$ very close to the real segment (0,1), where all the poles must lie. Since

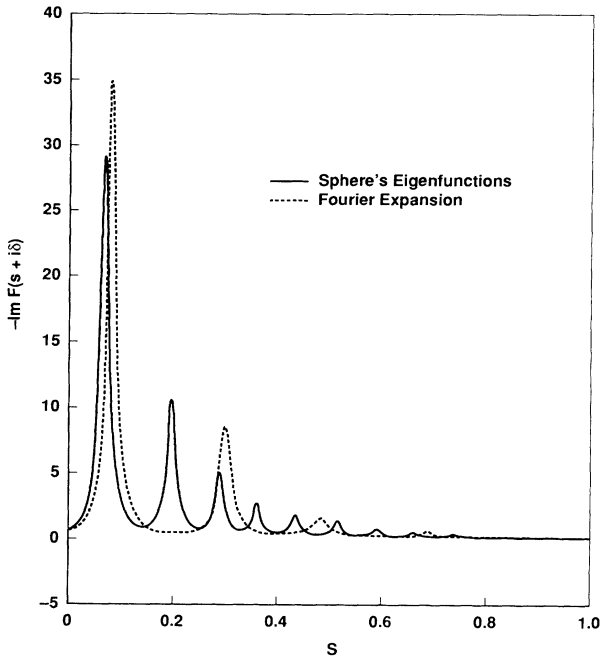

FIG. 2. Plot of $-\mathrm{Im}[F(s)]$ for s near the real segment [0,1]. The peaks indicate the positions of the poles, while the height of each peak is approximately 100 times the residue of that pole since we used $\delta = 0.01$.

the quantity

$$g(s) = -\lim_{\delta\to 0}\mathrm{Im}[F(s+i\delta)], \quad s\in(0,1) \tag{3.4}$$

is the spectral density of $F(s)$, an evaluation of $\mathrm{Im}[F(s+i\delta)]$ for sufficiently small δ will yield both the positions and the residues of all the poles. These will of course be the poles of the *approximant* we are using and *not* of the true $F(s)$. Nevertheless, if the approximation is a good one, we expect at least the poles with the largest residues to be calculated accurately. In Fig. 2 we plot the function $-\mathrm{Im}[F(s+i\delta)]$ for a fixed, small value of δ (i.e., $\delta=0.01$). The one computed by the Fourier expansion method using the linearly extrapolated μ_r is shown as a dashed curve, which indicates four distinct poles. This is

TABLE VII. Bounds on $F(s)$ for a simple cubic array of overlapping spheres for various values of s computed by the continued fraction method using Fourier expansion and linearly extrapolated zero moments of $C^{(r)}(s)$. $p_1=0.896$.

		$s=-0.1$ ($\epsilon_1/\epsilon_2=11$)		$s=-0.01$ ($\epsilon_1/\epsilon_2=101$)		$s=-0.001$ ($\epsilon_1/\epsilon_2=1001$)	
r	μ_r	Bound 1	Bound 2	Bound 1	Bound 2	Bound 1	Bound 2
0	0.895878	-8.958775	-4.388921	-89.58775	-7.850139	-895.8775	-8.522225
1	0.333333	-6.650539	-8.570771	-20.03864	-85.21682	-25.08934	-851.6081
2	0.672112	-8.425236	-7.660095	-83.27793	-35.94887	-831.6054	-57.09250
3	0.224360	-8.167319	-8.391430	-57.96513	-82.74522	-150.5240	-826.0059
4	0.575954	-8.371705	-8.276029	-82.36713	-67.62627	-821.9418	-246.2132
5	0.180717	-8.343658	-8.368229	-77.09291	-82.28626	-472.1905	-821.0530
6	0.375374	-8.364028	-8.351176	-82.15706	-78.54483	-819.5840	-538.8575
7	0.381287	-8.355990	-8.362334	-79.69177	-82.08179	-605.5187	-818.6863
8	0.214089	-8.359567	-8.356657	-81.84090	-79.88576	-815.4544	-618.5090
9	0.587693	-8.356994	-8.358374	-80.00220	-81.57654	-626.7029	-811.0242

TABLE VIII. Comparison of our results with those of Milton, McPhedran, and McKenzie (Ref. 13), Tao, Chen, and Sheng (Ref. 1), and Maxwell-Garnett for a 2D square array of prisms. $s=-0.25$, i.e., $\epsilon_1/\epsilon_2=5$.

p_1	Present method	Milton, McPhedran, and McKenzie	Tao, Chen, and Sheng	MG
0.1	1.1505	1.1490	1.1487	1.1429
0.2	1.3284	1.3239	1.3233	1.3077
0.3	1.5385	1.5359	1.5553	1.5000
0.4	1.8151	1.8079	1.7853	1.7273
0.5	2.2404	2.236	2.2327	2.0000

to be compared with that computed by expansion over the basis of sphere eigenfunctions, shown as a solid curve, which indicates nine distinct poles. The number of poles is approximately one-half of the number of μ_r's. Notice that the amplitude of the pole is F_n/δ and that the sum of the residues, as determined from this plot, is approximately 0.5, as it should be in this case.

B. Overlapping spheres and 2D prisms

Our results for three-dimensional simple cubic arrays of nonoverlapping and overlapping spheres are shown in Table VI along with the results of some previous studies.

Fourier-expansion calculations were performed for the first ten moments of $F(s)$ for reciprocal-lattice sizes of N up to 29 for the volume fraction $p_1=0.5$, of N up to 27 for $p_1=0.5236$ (when the spheres just touch each other), and of N up to 21 for all the other volume fractions. The function $F(s)$ was calculated by linearly extrapolating the zero moments of $C^{(r)}(s)$ of the two largest reciprocal lattices. As an illustration of how bounds get tighter for overlapping spheres, results for $p_1=0.896$ are shown in Table VII for various values of s. The last two columns in this table also illustrate the limitations of our method: When the contrast is huge, the upper and lower bounds do not approach each other very closely. In order to obtain tighter bounds for this case, one would not only have to calculate higher-order moments of $F(s)$, but one would also need to achieve much greater accuracy in the evaluation of its low-order moments.

We also computed the first ten moments of $F(s)$ for a two-dimensional square array of prisms and used them to calculate $F(s)$ at various values of s and p_1. Our calculations were performed for $N=18$ and 20, and $F(s)$ was estimated from its upper and lower bounds, computed by linear extrapolation of the $F(s)$ moments. In this 2D case, results obtained by extrapolating these moments seem to be better than those obtained by extrapolating μ_r. Results for $s=0.25$ are shown in Table VIII along with those of previous studies. Table IX shows more results from this calculation as compared to those of Ref. 13. The error bars represent the separation between the bounds. Table X indicates how our bounds for this case become tighter as more μ_r's are included in the calculation, and how they change when the contrast ϵ_1/ϵ_2 is increased.

IV. SUMMARY AND DISCUSSION

We have developed and implemented a Fourier-expansion method for calculating the bulk effective dielectric constant $\epsilon_e(\epsilon_1,\epsilon_2)$ of a two-component dielectric

TABLE IX. Comparison of our results with those of Milton, McPhedran, and McKenzie (Ref. 13) for a 2D square array of prisms. Each of our values was obtained as a simple average of the two bounds, and they also determined the quoted error. The drop in the size of the errors in the last row, in contrast with their previously established trend of increasing with row number, is associated with the fact that more of the moments μ_r were acceptable at the volume fraction $p_1 = 0.5$. This is one result of the numerical computations that we do not fully understand.

$p_1/(\epsilon_1/\epsilon_2)$	2	5	10	20	50	100
			Milton, McPhedran, and McKenzie			
0.1	1.0696	1.1490	1.1904	1.2162	1.2339	1.2402
0.2	1.1445	1.3239	1.4251	1.4910	1.5377	1.5548
0.3	1.2255	1.5359	1.7299	1.8654	1.9662	2.0039
0.4	1.3141	1.8079	2.1683	2.4518	2.6830	2.775
0.5	1.4142	2.236	3.162	4.47	7.07	10
			Present work			
0.1	1.0697	1.1505	1.1969	1.235±0.002	1.29±0.01	1.34±0.05
0.2	1.1447	1.3284	1.441±0.001	1.528±0.006	1.63±0.04	1.7±0.1
0.3	1.2254	1.5385	1.748±0.005	1.93±0.03	2.2±0.1	2.4±0.3
0.4	1.3144	1.8151	2.199±0.006	2.54±0.04	3.0±0.2	3.3±0.5
0.5	1.4142	2.2404	3.2105	4.766±0.001	8.87±0.01	15.4±0.2

TABLE X. Bounds on $F(s)$ for the 2D square array of prisms for various values of ϵ_1/ϵ_2 computed by the continued fraction method using Fourier expansion. $p_1=0.5$.

		$\epsilon_1/\epsilon_2=2$		$\epsilon_1/\epsilon_2=20$		$\epsilon_1/\epsilon_2=100$	
r	μ_r	Bound 1	Bound 2	Bound 1	Bound 2	Bound 1	Bound 2
0	0.500000	-0.500000	-0.333333	-9.500000	-0.904762	-49.50000	-0.980198
1	0.500000	-0.400000	-0.428571	-1.652174	-6.540984	-1.922330	-33.21927
2	0.500257	-0.416674	-0.411772	-5.203382	-2.225089	-25.24622	-2.811851
3	0.497867	-0.413811	-0.414652	-2.641877	-4.503306	-3.642817	-20.61720
4	0.500772	-0.414304	-0.414160	-4.104732	-2.930503	-17.62948	-4.401917
5	0.418275	-0.414231	-0.414256	-3.183338	-3.923749	-5.330279	-16.08206
6	0.501608	-0.414246	-0.414242	-3.802844	-3.334341	-14.88735	-6.126660
7	0.175081	-0.414245	-0.414245	-3.584779	-3.783298	-8.596538	-14.66976
8	0.506495	-0.414245	-0.414245	-3.767353	-3.657055	-14.47175	-9.986225
9	0.025621	-0.414245	-0.414245	-3.760483	-3.766988	-14.02300	-14.46677
10	0.722077	-0.414245	-0.414245	-3.766858	-3.765099	-14.46488	-14.33393

composite with a periodic microstructure. The method is applicable to *any* periodic microstructure, and it can provide very accurate results even in tough situations (i.e., high contrast ϵ_1/ϵ_2 and large volume fraction p_1) with but a moderate computing effort. This is borne out by the results we obtained for a number of different microstructures. In contrast with the Fourier expansion methods of Refs. 1 and 2, our method does not involve solving a large system of linear equations with a non-sparse matrix. For that reason our computations could be extended to reciprocal lattices of much larger sizes ($N=29$ as compared to $N=4$ and 5), resulting in a much greater accuracy.

Our approach is not restricted to calculations of ϵ_e (or analogous quantities like bulk effective conductivity σ_e) of two-component composites. It can be extended to a calculation of ϵ_e for multicomponent composites, and also to the calculation of the bulk effective elastic stiffness moduli of a periodic composite solid. These topics are currently being studied.

ACKNOWLEDGMENTS

One of us (DJB) has benefited from a conversation with B. U. Felderhof. This research was supported in part by the U.S.–Israel Binational Science Foundation under Grant No. 88-432, and in part by Chevron Oil Field Research Company.

[1] R. Tao, Z. Chen, and P. Sheng, Phys. Rev. B **41**, 2417 (1990).
[2] L. C. Shen, C. Liu, J. Korringa, and K. J. Dunn, J. Appl. Phys. **67**, 7071 (1990).
[3] J. W. S. Rayleigh, Philos. Mag. **34**, 481 (1892); also in *Scientific Papers of Lord Rayleigh* (Cambridge University Press, Glasgow, 1903), Vol. 4, p.19.
[4] R. C. McPhedran and D. R. McKenzie, Proc. R. Soc. London Ser. A **359**, 45 (1978).
[5] D. J. Bergman, J. Phys. C **12**, 4947 (1979).
[6] D. J. Bergman, in *Les Méthodes de l'Homogénéisation: Théorie et Applications en Physique* (École d'Été d'Analyse Numérique, Éditition Eyrolles, Paris, 1985), pp. 1–128.
[7] D. J. Bergman, Ann. Phys. **138**, 78 (1982).
[8] G. A. Baker, Jr., *Essentials of Padé Approximants* (Academic, New York, 1975), Chaps. 15 and 16.
[9] D. J. Bergman, in *Homogenization and Effective Moduli of Materials and Media*, edited by J. L. Ericksen, D. Kinderlehrer, R. Kohn, and J.-L. Lions (Springer-Verlag, New York, 1986), pp. 27–51.
[10] R. C. McPhedran and G. W. Milton, Appl. Phys. A **26**, 207 (1981).
[11] Z. Hashin and S. Shtrikman, J. Appl. Phys. **33**, 3125 (1962).
[12] R. Landauer, in *Electrical Transport and Optical Properties of Inhomogeneous Media*, edited by J. C. Garland and D. B. Tanner, AIP Conf. Proc. No. 40 (AIP, New York, 1978), p. 7; a complete set of earlier references can be found in this review article.
[13] G. W. Milton, R. C. McPhedran, and D. R. McKenzie, Appl. Phys. **25**, 23 (1981).